Volume 10 | Number 6 | 16 March 2026

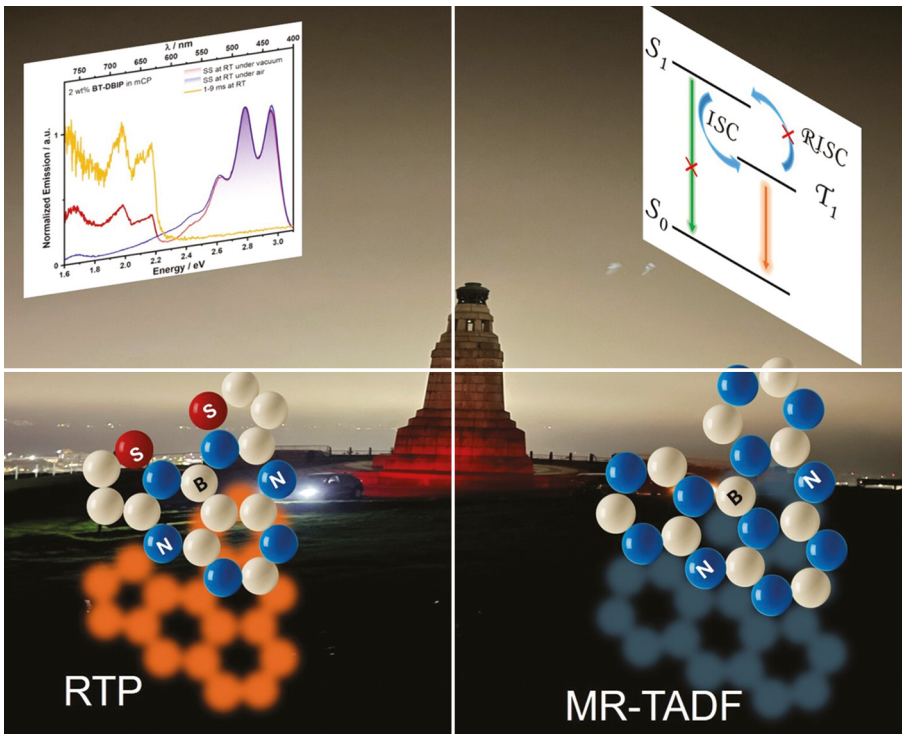

MATERIALS CHEMISTRY

FRONTIERS

CCS 中国化学会 CHINESE CHEMICAL SOCIETY
ICCAS 1956
ROYAL SOCIETY OF CHEMISTRY
rsc.li/frontiers-materials

MATERIALS CHEMISTRY FRONTIERS

RESEARCH ARTICLE

View Article Online
View Journal | View Issue

Cite this: *Mater. Chem. Front.*, 2026, **10**, 947

Room temperature phosphorescence from a benzothiophene-based N–B–N multi-resonance core

Durai Karthik, †‡ Abhishek Kumar Gupta ‡ and Eli Zysman-Colman *

Received 15th December 2025,
Accepted 23rd January 2026

DOI: 10.1039/d5qm00893j

rsc.li/frontiers-materials

We report a design strategy that enables room temperature phosphorescence from an N–B–N type heterocycle, reminiscent of a multi-resonance thermally activated delayed fluorescence (MR-TADF) compound, by disturbing the alternating frontier molecular orbital distribution pattern through five-membered ring fusion with the boron atom. The 2 wt% doped film in mCP host showed a long phosphorescence lifetime of 51.5 ms at 571 nm at room temperature, with an afterglow visible for up to 1 s.

Introduction

Room temperature phosphorescence (RTP) is a term that describes long-lived luminescence originating from the triplet excited state of organic compounds.[1–3] This radiative relaxation from the T_1 excited state to the S_0 ground state is formally a spin-forbidden transition. As spin–orbit coupling is generally weak in organic materials, the emission lifetime for this process is usually slow, ranging from microseconds to several seconds.[1,4–7] For RTP, population of the T_1 state must also occur following photoexcitation, and this too is only possible due to intersystem crossing from the singlet manifold being mediated by spin–orbit coupling (SOC) that is competitive with fast radiative decay in the form of fluorescence from the S_1 state. Unlike thermally activated delayed fluorescent materials, typically in RTP emitters, the energy gap between S_1 and T_1, ΔE_{ST}, is large, so reverse intersystem crossing is not competitive with phosphorescence.

Over the past decade, significant efforts have been made to increase the efficiency of RTP by enhancing SOC through either the incorporation of heavy p-block atoms such as sulfur[8–10] and/or the introduction of moieties that engineer the triplet excited state to have a different orbital type to both S_1 and S_0, such as the use of carbonyl groups.[11] Non-radiative decay of the triplet excitons competes with RTP. A number of strategies have been used to mitigate the non-radiative decay and thus enhance the efficiency of the RTP. These include crystallization,[12,13] host–guest interaction,[14,15] matrix rigidification,[16,17] molecular aggregation,[18–21] and co-crystallization.[22,23] However, these strategies are not conducive to employing these materials in an amorphous state, such as in thin films. So, engineering RTP from organic compounds in amorphous films remains a challenge.[24–26]

RTP can be turned on as a function of host medium. For instance, Yao *et al.* reported the narrowband RTP compound, **7MQ** (Fig. 1a). When **7MQ** is a dopant in benzophenone (BP) host, RTP is observed, whereas TADF is detected as a doped film in 9,9-(1,3-phenylene) bis-9*H*-carbazole (mCP) or bis[2-(diphenylphosphino)phenyl] ether oxide (DPEPO) hosts. The ΔE_{ST} of **7MQ** is 0.18 eV, which is sufficiently small to expect TADF.[27] However, the BP host acts as a triplet sensitizer, and triplet exciton transfer to **7MQ** occurs *via* Dexter energy transfer, resulting in RTP. In contrast, mCP and DPEPO act only as high triplet energy hosts, enabling FRET to **7MQ**, which then emits TADF. Another example comes from Du *et al.* who reported a series of cycloborylated thiabenzothiophene RTP emitters.[26] For example, the ΔE_{ST} of **α-DThBSS-Cz** is 0.48 eV, rendering reverse intersystem crossing (RISC) not thermally accessible; however, the four sulfur atoms enhance SOC ($T_1 \rightarrow S_0$ = 0.51 cm^{-1}) and are responsible for turning on RTP in these compounds, which the authors exploited as dyes for anti-counterfeiting technology. Recently, our group reported a series of nitrogen-containing indolocarbazoles, some of which (**6NICz** and **6,10NICz**) showed unusual biluminescence originating from RTP and TADF.[28] Very recently, Jang *et al.* reported a series of unsymmetrical narrowband fluorescent emitters, **BFD**, **BFD-Ph**, and **BFD-DTB**, featuring benzo[*b*]thiophene as a triplet exciton managing unit.[29] Despite having a structure that is reminiscent of an MR-TADF emitter skeleton, the **BFD** series exhibits neither TADF nor RTP; rather, these compounds are narrowband fluorescent. This is because the sulfur atom of the benzothiophene contributes to a stabilized T_1 level, resulting in large ΔE_{ST} of 0.38, 0.41, and 0.38 eV for **BFD**,

Organic Semiconductor Centre, EaStCHEM School of Chemistry, University of St Andrews, St Andrews, KY16 9ST, UK. E-mail: eli.zysman-colman@st-andrews.ac.uk
† Current address: Department of Chemistry, SRM Institute of Science and Technology, Kattankulathur – 603203, Tamil Nadu, India.
‡ These authors contributed equally.

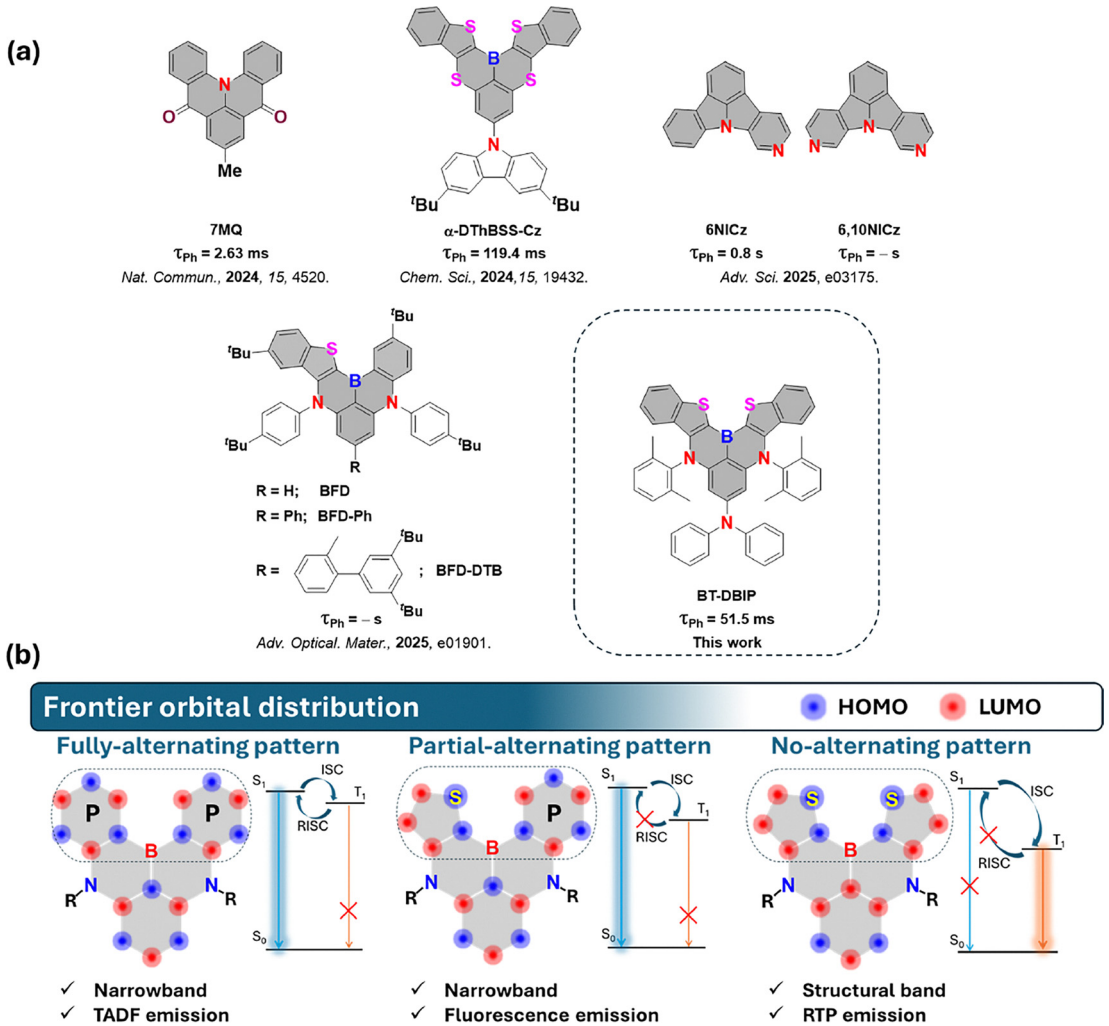

Fig. 1 (a) Molecular structures of selected reported RTP emitters and **BT-DBIP**, (b) frontier orbital distribution of distinct N–B–N cyclo-borylated skeletons with different electron density distribution patterns and the molecular design of this work, "P" indicates the phenyl ring involved in the cyclo-borylation.

BFD-Ph, and **BFD-DTB**, respectively, which renders TADF inaccessible at ambient temperatures. These molecules were employed as emitters in OLEDs, which exhibited a maximum external quantum efficiency, EQE_{max}, of 11.3%. Although these emitters are not exhibited TADF, the increase in EQE above 5% was ascribed by the authors as due to triplet–triplet annihilation (TTA), given the 3 wt% doping used in the device. All these results indicate that triplet excitons can be harvested either through their conversion to singlet excited states *via* TADF/TTA, or directly radiatively decaying *via* RTP. However, the molecular design strategy required to achieve pure RTP emission from molecules resembling an MR-TADF motif is not yet well understood.

It is interesting to cross-compare the HOMO and LUMO electron distribution arrangements in N–B–N MR-TADF motif, like in **DABNA-1**, with those in the **BFD** series of emitters (Fig. 1b). The cycloborylated benzothiophene ring exhibits a random HOMO and LUMO distribution, which disrupts the alternating pattern of the electron density distribution that is responsible for the short-range charge transfer (SRCT), producing compounds with much larger ΔE_{ST} and no TADF; notably, the two cycloborylated phenyl rings (P) display alternating HOMO and LUMO distributions. By considering these results, we envisaged that the formation of a stabilized triplet excited state, facilitated by a non-alternate HOMO and LUMO arrangement within an N–B–N MR motif would result in pure RTP emission.

Here, we report an organic RTP emitter, **BT-DBIP**, based on an unusual motif consisting of a cycloborylated benzothiophene (Fig. 1a). The structure is reminiscent of MR-TADF scaffolds but its emissive excited states are of locally excited character, not the required SRCT character that is characteristic of MR-TADF emitters. The cycloborylation to benzothiophene alters the HOMO and LUMO topologies, resulting in a large singlet–triplet gap, ΔE_{ST}, of 0.82 eV in 2 wt% doped films in mCP host, while the presence of two proximal sulfur atoms enhances, turning on RTP. We believe that this design offers valuable insight for the development of organic small-molecule RTP emitters.

Results and discussion

The target emitter **BT-DBIP** was synthesized in three steps as shown in Scheme 1. The synthesis began with a palladium-catalysed C–N coupling reaction between 2,6-dimethylaniline and 3-bromobenzothiophene to obtain intermediate **1** in 49% yield. Compound **1** was reacted with 3,5-dichloro-*N*,*N*-diphenylaniline in a second Buchwald–Hartwig cross-coupling to yield intermediate **2** in 84%. Electrophilic borylation of **2** with BBr_3 and di*iso*propylethylamine afforded **BT-DBIP** in 56% yield. The targeted emitter was characterized by ^1H and ^{13}C NMR spectroscopy, high-resolution mass spectrometry (HRMS), elemental analysis (EA), melting point determination, and high-performance liquid chromatography (HPLC) analysis (Fig. S1–S11). Thermal stability of **BT-DBIP** was evaluated by thermogravimetric analysis, **BT-DBIP** possesses a high thermal decomposition temperature (T_d) of 444 °C at 5% weight loss (Fig. S12).

Theoretical studies

We first modelled the optimized geometry and optoelectronic properties of **BT-DBIP** in the gas phase, starting from a structure obtained in Chem3D, using density functional theory (DFT) and time-dependent density functional theory (TD-DFT) at the PBE0/6-31G(d,p) level.[30,31] The frontier molecular orbitals, energy levels, and low-lying excited-state energies of **BT-DBIP** are shown in Fig. 2a and the optimized geometry is depicted in Fig. S13. The HOMO and LUMO are each distributed across the benzothiophene and central aryl-substituted rings, while there is no electron density on any of the peripheral amine groups in the HOMO and limited electron density on the peripheral diphenylamine nitrogen atom in the LUMO. The electron density distributions of the HOMO and LUMO do not alternate like typical MR-TADF molecules such as **PAB**[32] (Fig. S14). For instance, in **BT-DBIP**, there is a significant contribution to the HOMO from the *ortho*-sulfur atom relative to the boron atom. This is because the electron-rich sulfur atom influences the electron density distribution at this position, which decreases the LUMO contribution and increases the HOMO contribution. A typical MR-TADF material, such as **PAB**, has no contribution at the *ortho*-carbon position to boron in the HOMO, while in the LUMO, this contribution is large at this position.

The excited-state properties were calculated by using time-dependent density functional theory (TD-DFT) within the Tamm–Dancoff approximation (TDA-DFT) based on the optimized ground-state geometries at the same level of theory.[33,34] The calculated energy of the first singlet state (S_1) is 3.14 eV, and the first triplet (T_1) state is 2.43 eV, leading to a singlet–triplet energy gap, ΔE_{ST}, of 0.71 eV. This is too large for TADF to be operational. Natural transition orbital (NTO) analysis shows a significant hole (blue) density sited at the sulfur (Fig. 2b), while there is a much smaller particle (red) density contribution, which indicates that the sulfur atom makes the *ortho*-position electron richer (relative to boron) rather than electron-deficient. Thus, the hole and particle in the excited state do not show an alternating pattern that is consistent with an MR-TADF compound.[35] There is an intermediate T_2 state that lies between the S_1 and T_1 energy levels (0.71 eV), and so may contribute to any ISC/RISC processes. The spin–orbit coupling matrix element (SOCME) values between T_2 and S_1, T_2 and S_0, T_1 and S_1 and T_1 and S_0 were calculated at the same level of theory using the T_1 optimized geometry. The SOCME value of T_2–S_0 ($\langle S_0|H_{SO}|T_2\rangle$) is 0.97 cm^{-1}, which is higher than that for T_2–S_1 ($\langle S_1|H_{SO}|T_2\rangle$) of 0.41 cm^{-1}. There is a large SOCME value for T_1–S_0 ($\langle S_0|H_{SO}|T_1\rangle$) of 1.36 cm^{-1}, whereas the SOCME value between T_1–S_1 ($\langle S_1|H_{SO}|T_1\rangle$) of 0.08 cm^{-1} is small. The difference density plot of two lowest lying singlet and triplet excited states of **BT-DBIP** shows no alternating pattern of increasing electron density (red) and decreasing electron density (blue) (Fig. S14b), which implies that this state does not possess SRCT character. Taken together, the calculations predict that this compound is likely to be room temperature phosphorescent; note that the S_0–S_1 transition is predicted to be moderately strong, with an oscillator strength, *f*, of 0.33.

Electrochemistry

Cyclic voltammetry (CV) and differential pulse voltammetry (DPV) measurements in DCM with 0.1 M $[^nBu_4N]PF_6$ as the supporting electrolyte were used to infer the HOMO/LUMO levels of **BT-DBIP** (Fig. 3a). **BT-DBIP** possesses a reversible oxidation wave at E_{ox} at 0.83 V *vs.* SCE, which is assigned to the oxidation of the embedded amine units present in the cycloborylated motif.[29,32,36] The corresponding HOMO level is −5.15 eV. The HOMO level of **BT-DBIP** is destabilized compared to those of the **BFD** series (−5.42 eV to −5.46 eV),[29] the arylamine analogue **PAB** (−5.21 eV),[32] and the carbazole analogue **tDPA-DtCzB**[33] (−5.24 eV), reflecting the significant contribution from the electron-rich benzothiophene units to increase the HOMO level. No reduction was detected within the solvent window, so the LUMO level was estimated from the HOMO level and the optical band gap (E_{opt} = 3.03 eV), itself determined from the intersection of the normalized absorption and emission spectra in toluene (Fig. S15). The LUMO of **BT-DBIP** is thus at −1.68 eV.

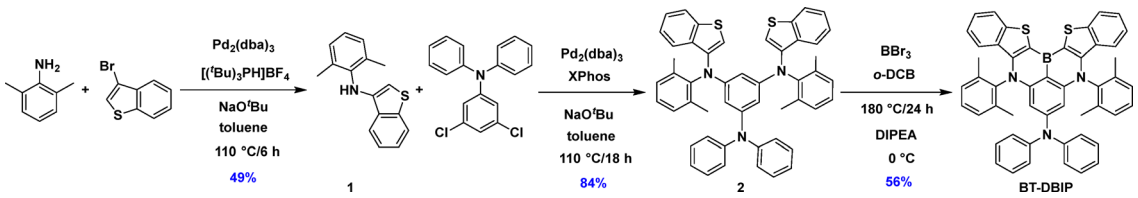

Scheme 1 Synthetic scheme of **BT-DBIP**.

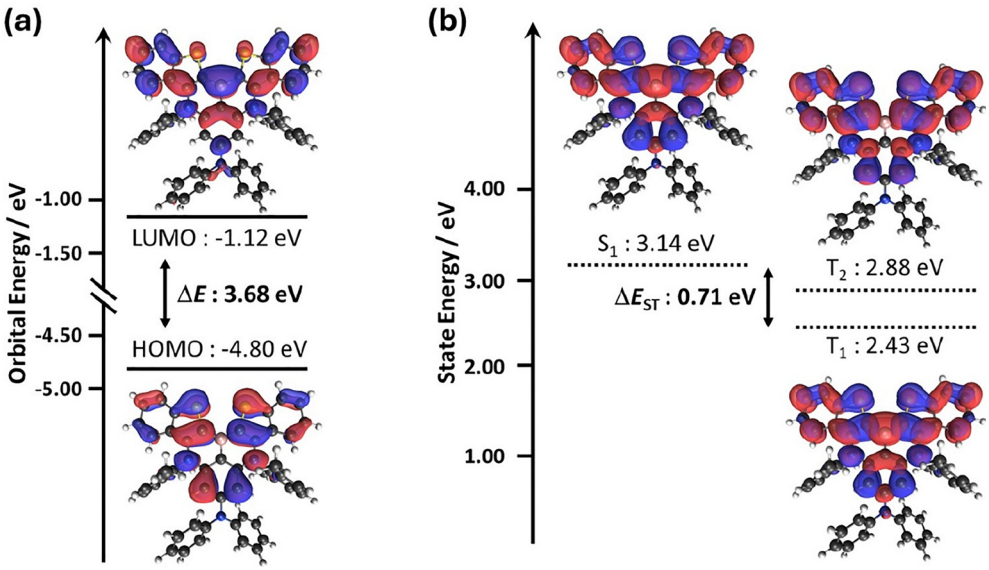

Fig. 2 (a) Frontier orbitals of **BT-DBIP** (isovalue of 0.02) and (b) natural transition orbitals (NTO) (isovalue of 0.02) of singlet (S_1) and triplet excited states (T_1 and T_2), hole (blue) and particle (red). All calculations at the PBE0/6-31G(d,p) level in the gas phase.

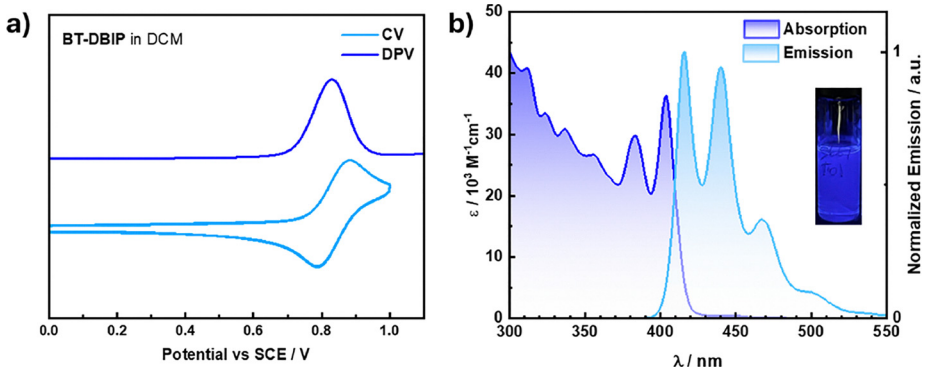

Fig. 3 (a) Cyclic and differential pulse voltammograms of **BT-DBIP** in degassed DCM with 0.1 M [^{n}Bu$_4$N]PF$_6$ as the supporting electrolyte and Fc/Fc$^+$ as the internal reference *versus* SCE (0.46 V *vs.* SCE)[37] (scan rate = 100 mV s^{-1}); (b) absorption and photoluminescence spectra of **BT-DBIP** in 1 × 10^{-5} M toluene (λ_{exc} = 374 nm), (inset: Picture of **BT-DBIP** in toluene solution under 364 nm excitation).

Photophysical studies

The photophysical properties of **BT-DBIP** were first measured in dilute toluene solution (Table 1 and Fig. 4b). There are two pronounced low-lying absorption bands at 385 and 404 nm, attributed to locally excited (LE) π–π* transitions based on TDA-DFT calculations (Table S2). The absorption spectrum of **BT-DBIP** is hypsochromically shifted by 55 nm compared to that of the structurally closely related compound, **α-DThBSS-Cz** (λ_{abs} = 459 nm),[26] indicating the absence of SRCT bands in the former. The molar absorptivity, ε, of the band at 404 nm in **BT-DBIP** (36.3 × 10^3 M^{-1} cm^{-1}) is larger than the lowest energy band at 459 nm in **α-DThBSS-Cz** (*ca.* 28 × 10^3 M^{-1} cm^{-1}), likely due to greater involvement of the diphenylamine unit, which increases the absorptivity for the LE transition in **BT-DBIP** compared to the more conformationally twisted ^{t}Cz group in **α-DThBSS-Cz.** The emission spectrum is a mirror image of the lowest energy part of the absorption spectrum and is structured, reflecting emission from a LE state. The PL peaks at λ_{PL} 416 nm and shows a vibronic progression with λ_{PL} of 440, 467, and 500 nm (Table 1). The Stokes shift is 12 nm (0.09 eV or 726 cm^{-1}, Fig. S15), and the FWHM is 53 nm (0.37 eV or 2984 cm^{-1}), the magnitude of both reflecting the rigid structure of this emitter. We calculated the Huang–Rhys (HR) factor as a function of the normal vibrational frequencies (cm^{-1}) in the gas phase to quantify the coupling strength between structural displacement and vibrational modes.[38] The vibrational mode analysis indicates that the low-frequency modes below 50 cm^{-1} (with HR factors of 0.24 at 37 cm^{-1}, 0.15 at 54 cm^{-1}, and 0.16 at 92 cm^{-1}), can be attributed to the twisting vibrations of the 2,6-dimethylaniline. In contrast, the high-frequency vibrational modes in the range of 1407–1675 cm^{-1} make significant contributions to the reorganization energies of **BT-DBIP**. These

Table 1 Photophysical properties of **BT-DBIP** in solution and thin film

Compound	Medium	λ_{abs}[c] /nm	λ_{PL}[d]/nm	FWHM[e]/nm	E_{S1}[f]/eV	E_{T1}[f]/eV	ΔE_{ST}[g]/eV	Φ_{PL}[h]/%	Φ_{Ph}[i]/%	τ_p[j]/ns	τ_d[j]/ms
BT-DBIP	Sol.[a]	404	416, 440, 467	53	3.07	2.23	0.84	32.8/26.5	6.3	3.13	—
	Film[b]	—	420, 445, 473 (550, 571, 627)	—	3.03	2.21	0.82	8.7/5.0	3.7	2.87	51.5/46.3

[a] In toluene solutions (10^{-5} M). [b] Spin-coated thin films consisting of 2 wt% **BT-DBIP** in mCP under vacuum, λ_{exc} = 340 nm. [c] Lowest energy absorbance band. [d] Steady-state PL maximum at 300 K, λ_{exc} = 374 nm for solution and 340 nm for thin film. The values in parentheses are when the sample is under vacuum. [e] Full-width at half maximum of PL peak. [f] S_1 and T_1 energies obtained from the onsets of the respective steady-state PL at 77 K (prompt) and delayed emission spectra (delay: 1 ms; gate time: 9 ms) at 77 K (λ_{exc} = 374 nm for glassy 2-MeTHF and 340 nm for thin film). [g] in 2-MeTHF (10^{-6} M), $\Delta E_{ST} = E(S_1) - E(T_1)$. [h] Photoluminescence quantum yields (Φ_{PL}) of **BT-DBIP** measured by a relative method using quinine sulfate as the reference (Φ_{PL} = 54.6% in 1 N H_2SO_4) in optically dilute solutions in toluene under degassed/aerated conditions.[39] Absolute Φ_{PL} of the thin films measured using an integrating sphere under degassed/aerated conditions. [i] The Φ_{Ph} is calculated by subtracting the Φ_{PL} in air from the Φ_{PL} under N_2. [j] Prompt and delayed PL lifetimes were obtained by TCSPC (λ_{exc} = 375 nm) and MCS (at λ_{PL} of 571/627 nm, λ_{exc} = 340 nm), respectively.

modes are primarily dominated by the stretching and scissoring vibrations of the B–C–S bonds of the cyclo-borylated benzothiophene rings (Fig. S16). Fig. 4a shows the steady-state PL spectra in 2-MeTHF at RT and at 77 K, and the delayed emission spectrum (gated emission, 1–9 ms acquisition window) at 77 K. The steady-state PL spectrum closely aligns with that at 77 K, indicating emission from the same LE state. The phosphorescence spectrum is also structured, peaking at 562 and 616 nm. The onset of the steady-state PL spectrum at 77 K provides an estimate of the S_1 energy, whereas the onset of the gated emission spectrum at 77 K relates to the energy of the T_1 state. The S_1 and T_1 energies are 3.07 eV and 2.23 eV, respectively, and the ΔE_{ST} is 0.84 eV, which is much higher than the ΔE_{ST} (0.48 eV) of **α-DThBSS-Cz** (Table 1). The large ΔE_{ST} indicates that TADF is almost certainly not operational, and this aligns with the DFT study. The solvatochromism study (Fig. S17 and Table S1) corroborates the assignment of a LE character to the emissive excited state, as there is only a slight spectral red-shifting and broadening. Time-resolved PL measurements in toluene at room temperature under vacuum showed a monoexponential decay of the emission, with a PL lifetime, τ_{PL}, of 3.13 ns, there was no delayed emission detected (Fig. S18). The photoluminescence quantum yield (Φ_{PL}) of **BT-DBIP** in degassed toluene is 33%, which decreases to 27% upon exposure to air. The PL spectra of degassed and aerated solutions of **BT-DBIP** in toluene (Fig. S19) likewise reveal a quenching in the presence of O_2. These studies suggest that there are triplet excited states that are being populated upon photoexcitation. The phosphorescence quantum yield (Φ_{Ph}) is 6.3% in toluene.

We next evaluated the photophysical properties of **BT-DBIP** as a 2 wt% doped film in 1,3-bis(*N*-carbazolyl)benzene (mCP). The steady-state PL spectrum under air is similar to that measured in toluene, peaking at λ_{PL} of 420 nm, with major vibrational bands at 445, 473, and 506 nm (Table 1 and Fig. 4b). When the sample is placed under vacuum, a second lower-energy structured emission appears at λ_{PL} 550 nm (with bands also at 571 and 627 nm) that we assign to RTP. The room temperature gated emission spectrum (1–9 ms acquisition) under vacuum corroborates the assignment of the low-energy emission to phosphorescence. The Φ_{PL} of **BT-DBIP** is 8.7%, which decreased to 5.0% upon exposure to air (Table 1). Thus, the calculated Φ_{Ph} of **BT-DBIP** is 3.7%.

Temperature-dependant gated emission spectra under vacuum (Fig. 4c) document that the phosphorescence intensity increases with decreasing temperature, reflecting the suppression of non-radiative decay pathways at lower temperatures. The measured S_1 and T_1 energies of the 2 wt% doped film of **BT-DBIP** are 3.03 and 2.21 eV, and the ΔE_{ST} is 0.82 eV, values that are very similar to those measured in glassy 2-MeTHF (Fig. 4c). The time-resolved PL decays were measured at each of λ_{PL} of 420, 445, 571, and 627 nm under vacuum at RT. At 420 and 445 nm, the

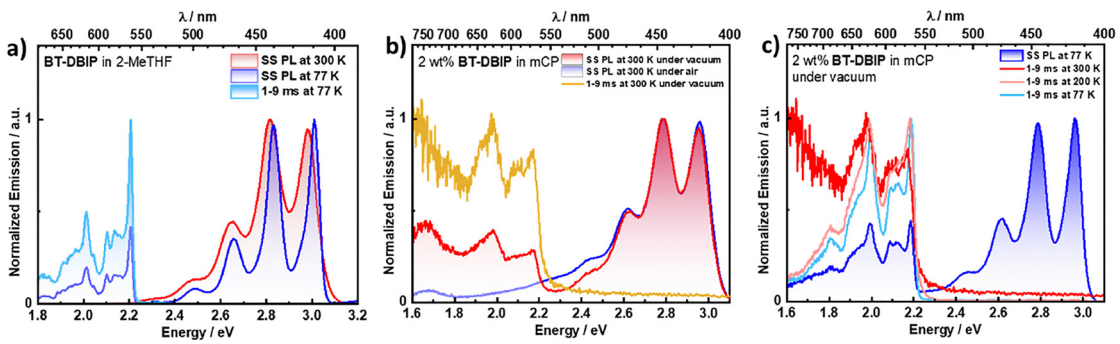

Fig. 4 (a) Steady-state fluorescence PL (SS PL) spectra at room temperature and 77 K and phosphorescence spectrum (acquisition time range of 1–9 ms) at 77 K of **BT-DBIP** in 2-MeTHF (λ_{exc} = 374 nm); (b) steady-state PL spectra SS PL at 300 K under vacuum and air and phosphorescence spectrum (acquisition time range of 1–9 ms) at 300 K of 2 wt% doped film of **BT-DBIP** in mCP (λ_{exc} = 340 nm); (c) steady-state PL spectrum SS PL at 77 K and phosphorescence spectra (acquisition time range of 1–9 ms) at 300, 200, and 77 K of 2 wt% doped film of **BT-DBIP** in mCP (λ_{exc} = 340 nm).

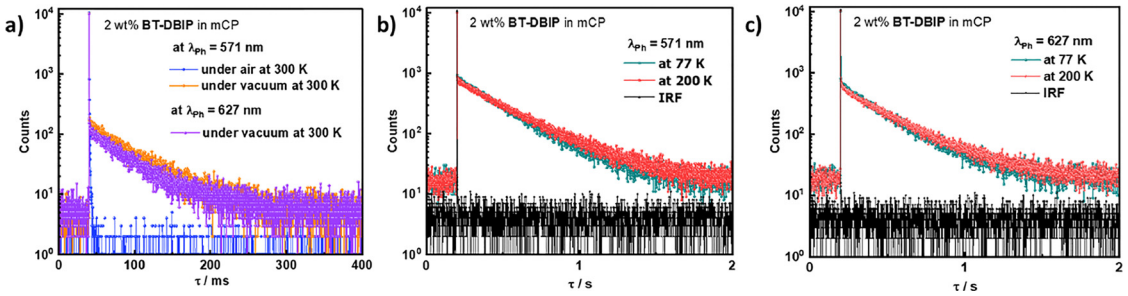

Fig. 5 (a) Time-resolved PL decays of 2 wt% doped film of **BT-DBIP** in mCP under air and vacuum at 300 K for λ_{PL}= 571 nm and λ_{PL}= 627 nm (λ_{exc}= 340 nm); (b) temperature-dependent time-resolved PL decays of 2 wt% doped film of **BT-DBIP** in mCP for λ_{PL} = 571 nm (λ_{exc}= 340 nm); (c) temperature-dependent time-resolved PL decays of 2 wt% doped film of **BT-DBIP** in mCP for λ_{PL} = 627 nm (λ_{exc}= 340 nm).

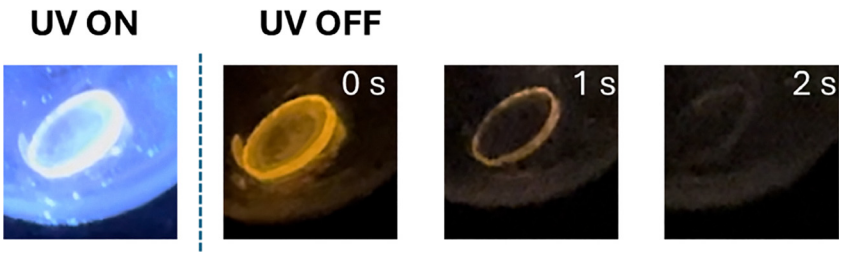

Fig. 6 Photos of 2.0 wt% doped film of **BT-DBIP** in mCP at room temperature under vacuum with and without UV irradiation (λ_{exc} = 365 nm). The times represent the delay after the excitation source was turned off.

emission decays with similar bi-exponential kinetics, with $\tau_{PL,avg}$ of 2.87 ns (Fig. S20). At 571 and 627 nm, the emission decays with similar monoexponential kinetics, with τ_{PL} of 51.5 and 46.3 ms, respectively. This long-lived emission is completely quenched upon exposure to air (Fig. 5a). The τ_{PL} increases to 269.74 ms at 200 K and to 309.1 ms at 77 K (detecting at λ_{PL} of 571 nm, Fig. 5b and Fig. S21), while similarly the τ_{PL} increased to 258.0 ms at 200 K and to 289.5 ms at 77 K (detecting at λ_{PL} of 627 nm, Fig. 5c). This behavior is consistent with the temperature-dependent steady-state PL data. Indeed, the RTP emission (λ_{exc} = 365 nm) from the 2 wt% doped film in mCP under vacuum was observed for up to one second after the UV irradiation (Fig. 6).

Conclusions

A new RTP emitter **BT-DBIP** was developed by incorporating benzothiophene segment within a prototypical boron-based MR-TADF skeleton. Calculations showed that the alternating frontier molecular orbitals are disturbed by the five-membered ring at the cycloborylated benzothiophene core, resulting in LE emission rather than emission from a SRCT state. The presence of sulfur atoms in **BT-DBIP** increases SOC between S_1 and T_1 and T_1 and S_0, enhancing both ISC and phosphorescence rates. Because of the rigid molecular structure, the PL spectrum of **BT-DBIP** in toluene is structured, and the Stokes shift is small. The 2 wt% doped film of **BT-DBIP** in mCP likewise showed RTP in the absence of air, with a phosphorescence lifetime of 51.5 ms. This work demonstrates a design concept to develop RTP emitters based on perturbing the chemical structure of an N–B–N type MR-TADF skeleton.

Author contributions

D. K.: conceptualization, synthesis, investigation, writing–original draft preparation, review & editing. A. K. G.: data curation, formal analysis, investigation, theoretical and photophysical studies, writing – review & editing. E. Z-C.: project management, supervision, resources, writing–review & editing.

Conflicts of interest

There are no conflicts to declare.

Data availability

The research data supporting this publication can be accessed at **https://doi.org/10.17630/35824801-2ed5-458d-a7d8-2fd3a1593f27**.

Supplementary information (SI): ^{1}H NMR and ^{13}C NMR spectra, HRMS and HPLC; supplementary computational data and coordinates; additional photophysical data are available. See DOI: **https://doi.org/10.1039/d5qm00893j**.

Acknowledgements

We thank Gavin Peters for performing TGA and DSC experiments. We thank Samsung Display Co., Ltd., the Leverhulme

Trust (RPG-2022-032), and the Engineering and Physical Sciences Research Council for support (EP/R035164/1, EP/W007517/1, EP/Z535291/1).

References

1 W. Zhao, Z. He and B. Z. Tang, Room-temperature phosphorescence from organic aggregates, *Nat. Rev. Mater.*, 2020, **5**, 869–885.
2 H. E. Hackney and D. F. Perepichka, Recent advances in room temperature phosphorescence of crystalline boron containing organic compounds, *Aggregate*, 2022, **3**, e123.
3 Z. Wu, J. Nitsch and T. B. Marder, Persistent Room-Temperature Phosphorescence from Purely Organic Molecules and Multi-Component Systems, *Adv. Opt. Mater.*, 2021, **9**, 2100411.
4 X. Yang, G. I. N. Waterhouse, S. Lu and J. Yu, Recent advances in the design of afterglow materials: mechanisms, structural regulation strategies and applications, *Chem. Soc. Rev.*, 2023, **52**, 8005–8058.
5 Kenry, C. Chen and B. Liu, Enhancing the performance of pure organic room-temperature phosphorescent luminophores, *Nat. Commun.*, 2019, **10**, 2111.
6 W.-L. Zhou, W. Lin, Y. Chen and Y. Liu, Supramolecular assembly confined purely organic room temperature phosphorescence and its biological imaging, *Chem. Sci.*, 2022, **13**, 7976–7989.
7 Y. Gong, J. Yang, M. Fang and Z. Li, Room-temperature phosphorescence from metal-free polymer-based materials, *Cell Rep. Phys. Sci.*, 2022, **3**, 100663.
8 J. Yang, H. Gao, Y. Wang, Y. Yu, Y. Gong, M. Fang, D. Ding, W. Hu, B. Z. Tang and Z. Li, The odd–even effect of alkyl chain in organic room temperature phosphorescence luminogens and the corresponding in vivo imaging, *Mater. Chem. Front.*, 2019, **3**, 1391–1397.
9 Z. Xu, Q. T. Liu, X. Wang, Q. Liu, D. Hean, K. C. Chou and M. O. Wolf, Quinoline-containing diarylethenes: bridging between turn-on fluorescence, RGB switching and room temperature phosphorescence, *Chem. Sci.*, 2020, **11**, 2729–2734.
10 T. Wang, J. De, S. Wu, A. K. Gupta and E. Zysman-Colman, Thermally Activated and Aggregation-Regulated Excitonic Coupling Enable Emissive High-Lying Triplet Excitons, *Angew. Chem., Int. Ed.*, 2022, **61**, e202206681.
11 T. Wang, A. K. Gupta, D. B. Cordes, A. M. Z. Slawin and E. Zysman-Colman, Reducing Efficiency Roll-Off in Multi-Resonant Thermally Activated Delayed Fluorescent OLEDs through Modulation of the Energy of the T2 State, *Adv. Opt. Mater.*, 2023, **11**, 2300114.
12 T. Ono, K. Kimura, M. Ihara, Y. Yamanaka, M. Sasaki, H. Mori and Y. Hisaeda, Room-Temperature Phosphorescence Emitters Exhibiting Red to Near-Infrared Emission Derived from Intermolecular Charge-Transfer Triplet States of Naphthalenediimide–Halobenzoate Triad Molecules, *Chem. – Eur. J.*, 2021, **27**, 9535–9541.
13 H. Shi, L. Zou, K. Huang, H. Wang, C. Sun, S. Wang, H. Ma, Y. He, J. Wang, H. Yu, W. Yao, Z. An, Q. Zhao and W. Huang, A Highly Efficient Red Metal-free Organic Phosphor for Time-Resolved Luminescence Imaging and Photodynamic Therapy, *ACS Appl. Mater. Interfaces*, 2019, **11**, 18103–18110.
14 S. Iwakiri, R. Hasegawa and Y. Kubo, Near-Infrared Room-Temperature Phosphorescence in Arylselanyl BODIPY-Doped Materials, *ChemPhotoChem*, 2022, **6**, e202200073.
15 F. Xiao, H. Gao, Y. Lei, W. Dai, M. Liu, X. Zheng, Z. Cai, X. Huang, H. Wu and D. Ding, Guest-host doped strategy for constructing ultralong-lifetime near-infrared organic phosphorescence materials for bioimaging, *Nat. Commun.*, 2022, **13**, 186.
16 D. Lee, O. Bolton, B. C. Kim, J. H. Youk, S. Takayama and J. Kim, Room Temperature Phosphorescence of Metal-Free Organic Materials in Amorphous Polymer Matrices, *J. Am. Chem. Soc.*, 2013, **135**, 6325–6329.
17 M. Louis, H. Thomas, M. Gmelch, A. Haft, F. Fries and S. Reineke, Blue-Light-Absorbing Thin Films Showing Ultralong Room-Temperature Phosphorescence, *Adv. Mater.*, 2019, **31**, 1807887.
18 X. Sun, X. Wang, X. Li, J. Ge, Q. Zhang, J. Jiang and G. Zhang, Polymerization-Enhanced Intersystem Crossing: New Strategy to Achieve Long-Lived Excitons, *Macromol. Rap. Commun.*, 2015, **36**, 298–303.
19 E. Lucenti, A. Forni, C. Botta, L. Carlucci, C. Giannini, D. Marinotto, A. Pavanello, A. Previtali, S. Righetto and E. Cariati, Cyclic Triimidazole Derivatives: Intriguing Examples of Multiple Emissions and Ultralong Phosphorescence at Room Temperature, *Angew. Chem., Int. Ed.*, 2017, **56**, 16302–16307.
20 J. Yang, X. Zhen, B. Wang, X. Gao, Z. Ren, J. Wang, Y. Xie, J. Li, Q. Peng, K. Pu and Z. Li, The influence of the molecular packing on the room temperature phosphorescence of purely organic luminogens, *Nat. Commun.*, 2018, **9**, 840.
21 Z. Yang, Z. Mao, X. Zhang, D. Ou, Y. Mu, Y. Zhang, C. Zhao, S. Liu, Z. Chi, J. Xu, Y.-C. Wu, P.-Y. Lu, A. Lien and M. R. Bryce, Intermolecular Electronic Coupling of Organic Units for Efficient Persistent Room-Temperature Phosphorescence, *Angew. Chem., Int. Ed.*, 2016, **55**, 2181–2185.
22 L. Xiao, Y. Wu, Z. Yu, Z. Xu, J. Li, Y. Liu, J. Yao and H. Fu, Room-Temperature Phosphorescence in Pure Organic Materials: Halogen Bonding Switching Effects, *Chem. – Eur. J.*, 2018, **24**, 1801–1805.
23 M.-P. Zhuo, Y. Yuan, Y. Su, S. Chen, Y.-T. Chen, Z.-Q. Feng, Y.-K. Qu, M.-D. Li, Y. Li, B.-W. Hu, X.-D. Wang and L.-S. Liao, Segregated Array Tailoring Charge-Transfer Degree of Organic Cocrystal for the Efficient Near-Infrared Emission beyond 760 nm, *Adv. Mater.*, 2022, **34**, 2107169.
24 D. Li, F. Lu, J. Wang, W. Hu, X.-M. Cao, X. Ma and H. Tian, Amorphous Metal-Free Room-Temperature Phosphorescent Small Molecules with Multicolor Photoluminescence via a Host–Guest and Dual-Emission Strategy, *J. Am. Chem. Soc.*, 2018, **140**, 1916–1923.
25 D. Guo, W. Wang, K. Zhang, J. Chen, Y. Wang, T. Wang, W. Hou, Z. Zhang, H. Huang, Z. Chi and Z. Yang,

Visible-light-excited robust room-temperature phosphorescence of dimeric single-component luminophores in the amorphous state, *Nat. Commun.*, 2024, **15**, 3598.

26 B. Du, Y. Wu, X. Wang, H. Tian, S. Shao and L. Wang, Multi-resonance emitters with room-temperature phosphorescence in amorphous state and excited by visible light, *Chem. Sci.*, 2024, **15**, 19432–19442.

27 J. M. Dos Santos, D. Hall, B. Basumatary, M. Bryden, D. Chen, P. Choudhary, T. Comerford, E. Crovini, A. Danos, J. De, S. Diesing, M. Fatahi, M. Griffin, A. K. Gupta, H. Hafeez, L. Hämmerling, E. Hanover, J. Haug, T. Heil, D. Karthik, S. Kumar, O. Lee, H. Li, F. Lucas, C. F. R. Mackenzie, A. Mariko, T. Matulaitis, F. Millward, Y. Olivier, Q. Qi, I. D. W. Samuel, N. Sharma, C. Si, L. Spierling, P. Sudhakar, D. Sun, E. Tankelevičiūtė, M. Duarte Tonet, J. Wang, T. Wang, S. Wu, Y. Xu, L. Zhang and E. Zysman-Colman, The Golden Age of Thermally Activated Delayed Fluorescence Materials: Design and Exploitation, *Chem. Rev.*, 2024, **124**, 13736–14110.

28 O. S. Lee, A. P. McKay, D. B. Cordes, S. L. Warriner, M. C. Gather and E. Zysman-Colman, Simultaneous Multi-Resonant Thermally Activated Delayed Fluorescence and Room Temperature Phosphorescence from Biluminescent Nitrogen-Containing Indolocarbazoles, *Adv. Sci.*, 2025, **12**, e03175.

29 J. M. Jang, D. Lee, J. Moon and J. Y. Lee, Narrow-Emitting Multiple-Resonance Fluorescent Emitters with Deactivated Thermally Activated Delayed Fluorescence Mechanism Using Benzo[b]thiophene as a Triplet Energy Managing Unit, *Adv. Opt. Mater.*, 2025, **13**, e01901.

30 C. Adamo and V. Barone, Toward reliable density functional methods without adjustable parameters: The PBE0 model, *J. Chem. Phys.*, 1999, **110**, 6158–6170.

31 D. Hall, J. C. Sancho-García, A. Pershin, D. Beljonne, E. Zysman-Colman and Y. Olivier, Benchmarking DFT Functionals for Excited-State Calculations of Donor–Acceptor TADF Emitters: Insights on the Key Parameters Determining Reverse Inter-System Crossing, *J. Phys. Chem. A*, 2023, **127**, 4743–4757.

32 Y. Wang, Y. Duan, R. Guo, S. Ye, K. Di, W. Zhang, S. Zhuang and L. Wang, A periphery cladding strategy to improve the performance of narrowband emitters, achieving deep-blue OLEDs with CIEy < 0.08 and external quantum efficiency approaching 20%, *Org. Electron.*, 2021, **97**, 106275.

33 S. Grimme, Density functional calculations with configuration interaction for the excited states of molecules, *Chem. Phys. Lett.*, 1996, **259**, 128–137.

34 S. Hirata and M. Head-Gordon, Time-dependent density functional theory within the Tamm–Dancoff approximation, *Chem. Phys. Lett.*, 1999, **314**, 291–299.

35 A. Pershin, D. Hall, V. Lemaur, J.-C. Sancho-Garcia, L. Muccioli, E. Zysman-Colman, D. Beljonne and Y. Olivier, Highly emissive excitons with reduced exchange energy in thermally activated delayed fluorescent molecules, *Nat. Commun.*, 2019, **10**, 597.

36 X. Yan, Z. Li, Q. Wang, Y. Qu, Y. Xu and Y. Wang, Achieving highly efficient narrowband sky-blue electroluminescence with alleviated efficiency roll-off by molecular-structure regulation and device-configuration optimization, *J. Mater. Chem. C*, 2022, **10**, 15408–15415.

37 V. V. Pavlishchuk and A. W. Addison, Conversion constants for redox potentials measured versus different reference electrodes in acetonitrile solutions at 25 °C, *Inorg. Chim. Acta*, 2000, **298**, 97–102.

38 Z. Shuai, Thermal Vibration Correlation Function Formalism for Molecular Excited State Decay Rates, *Chin. J. Chem.*, 2020, **38**, 1223–1232.

39 W. H. Melhuish, Quantum efficiencies of fluorescence of organic substances: Effect of solvent and concentration of the fluorescent solute[1], *J. Phys. Chem.*, 1961, **65**, 229–235.

